

# Analyst

Accepted Manuscript



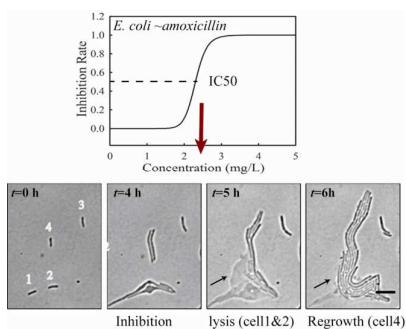
This is an *Accepted Manuscript*, which has been through the Royal Society of Chemistry peer review process and has been accepted for publication.

*Accepted Manuscripts* are published online shortly after acceptance, before technical editing, formatting and proof reading. Using this free service, authors can make their results available to the community, in citable form, before we publish the edited article. We will replace this *Accepted Manuscript* with the edited and formatted *Advance Article* as soon as it is available.

You can find more information about *Accepted Manuscripts* in the [Information for Authors](#).

Please note that technical editing may introduce minor changes to the text and/or graphics, which may alter content. The journal's standard [Terms & Conditions](#) and the [Ethical guidelines](#) still apply. In no event shall the Royal Society of Chemistry be held responsible for any errors or omissions in this *Accepted Manuscript* or any consequences arising from the use of any information it contains.

1  
2  
3 A new form of bacterial persistence was observed. Normal *E. coli* cells inhibited  
4 by amoxicillin recovered from the killing process when they had an opportunity  
5 to utilize the cytoplasm released from lysed cells close-by.  
6  
7



1  
2  
3 **1 Single cell growth rate and morphological dynamics revealing an “opportunistic”**  
4 **2 persistence**

5  
6 *Bing Li<sup>1</sup>, Yong Qiu<sup>1,\*</sup>, Andrew Glidle<sup>2</sup>, Jon Cooper<sup>2</sup>, Han-chang Shi<sup>1</sup> and HuaBing Yin<sup>2,\*</sup>*  
7

8  
9 <sup>1</sup> Environmental Simulation and Pollution Control State-key Joint Laboratory, School of Environment,  
10 Tsinghua University, Beijing 100084, China

11 <sup>2</sup> Division of Biomedical Engineering, School of Engineering, University of Glasgow, Glasgow G12 8LT,  
12 U.K.

13 \*Corresponding authors: [qiyong@tsinghua.edu.cn](mailto:qiyong@tsinghua.edu.cn) and [huabing.yin@glasgow.ac.uk](mailto:huabing.yin@glasgow.ac.uk)  
14

15 **ABSTRACT**

16 Bacteria persistence is a well-known phenomenon, where a small fraction of cells in an  
17 isogenic population are able to survive high doses of antibiotic treatment. Since the  
18 persistence is often associated with single cell behaviour, the ability to study the dynamic  
19 response of individual cells to antibiotics is critical.

20 In this work, we developed a gradient microfluidic system that enables long-term tracking  
21 of single cell morphology under a wide range of inhibitor concentrations. From time-lapse  
22 images, we calculated bacterial growth rates based on the variations in cell mass and in cell  
23 number. Using *E. coli* and *Comamonas denitrifican* to amoxicillin inhibition as model  
24 systems, we found the IC50 determined via both methods are in a good agreement.

25 Importantly, the growth rates together with morphological dynamics of individual cells has  
26 led to the discovery of a new form of persistence to amoxicillin. Normal cells that are  
27 sensitive to amoxicillin gain persistence or recover from the killing process, if they have had  
28 an opportunity to utilise the cytoplasm released from lysed cells close-by. We term this  
29 acquired persistence in normal growing cells “opportunistic persistence”. This finding might  
30 shed new insights into biofilm resistance and the effect of antibiotics on environmental  
31 microbes.  
32

33 **KEYWORDS**

34 Bacterial persistence, biofilm, microfluidics, antibiotics, single cell tracking,  
35 morphology.  
36  
37  
38  
39  
40  
41  
42  
43  
44  
45  
46  
47  
48  
49  
50  
51  
52  
53  
54  
55  
56  
57  
58  
59  
60

## INTRODUCTION

Bacterial persistence has been well known since 1940s when it was found that high doses of antibiotics were unable to kill all the cells in an isogenic population - a small fraction of cells “persist”.<sup>1</sup> When recultured, these persister bacteria regrew to form a similarly isogenic population that likewise could not be completely killed. In recent years, this situation has been compounded by the intensive use of antibiotics which has led to widespread bacterial resistance. This is becoming a serious threat to public health.<sup>2-4</sup> Furthermore, the rapid accumulation of antibiotics in the environment is now imposing a dramatically increasing stress on nature’s microbes.

Currently, conventional bacterial growth inhibition tests are commonly used as a standard measure of the adverse effects of antibiotics. Two widely used methods include optical density (OD) measurement<sup>5-7</sup> and plate dilution methods.<sup>8</sup> The former is an indirect measure of cell density, based on the assumption that cell dry mass is proportional to light absorbance, whereas the latter counts the viability of cells. Both methods quantify the antibiotic potency as the half maximal inhibitory concentration (IC<sub>50</sub>)<sup>9</sup> or minimum inhibitory concentration (MIC)<sup>10</sup>. However, discrepancies in growth parameters derived from two methods exist and are dependent on bacteria species and culture conditions.<sup>11-13</sup> Furthermore, both methods are end-point measurements, and involve manual operation. This significantly limits their use for investigating heterogeneous responses to antibiotic stress,<sup>14</sup> especially in respect of subpopulations, such as persister cells, whose formation changes in a fluctuating environment.<sup>15</sup>

Microfluidics has become an attractive tool for single cell analysis.<sup>16-20</sup> Trapping bacterial cells on chip using geometrical barriers<sup>15, 20, 21</sup> or with agarose gel<sup>22</sup> has been demonstrated, allowing time-lapse observations of single cells. Through *in situ* tracking of growth rates of individual cells, persister cells were identified from normal growing cells.<sup>15</sup> The powerful capability of microfluidics in controlling microflows have been explored in many cases, including the creation of a single cell chemostat,<sup>23</sup> programmable delivery of culture medium<sup>15</sup>, and the generation of concentration gradients for various investigations.<sup>24-26</sup>

Recently, we have developed a simple, gradient microfluidic system for rapid bacterial growth inhibition testing.<sup>27</sup> It employs the assembly of a polydimethylsiloxane (PDMS) chip and a thin agarose membrane to establish steady concentration gradients of inhibitors over a monolayer of bacteria. The system enables long-term tracking of morphological dynamics of individual bacteria under a wide range of inhibitor concentrations.

In this report we first illustrate this method using a model system with *Escherichia coli* (*E. coli*) and amoxicillin. We calculated bacterial growth rates based on the variations in cell mass and in cell number, and evaluated their effectiveness for assessing antibiotic inhibition potency. The growth rates, together with morphological dynamics of individual cells, were used to quantitatively evaluate individual responses to the stress. This led to the discovery of a new form of persistence in the amoxicillin killing process. Interestingly, the behaviour was also found in a naturally occurring bacteria *Comamonas denitrifican* - an environmental denitrifying bacterium.

## MATERIALS AND METHODS

### Microfluidic chip for single-layer cell culture

1  
2  
3 79 The microfluidic device developed in this study is shown in Figure 1. It contains an assembly  
4 80 of a coverslip glass, a thin agarose gel membrane and a PDMS chip (Figure 1). A monolayer  
5 81 of bacteria were trapped and grew between the agarose membrane and the coverslip. The  
6 82 PDMS chip was made by replica moulding as follows. Briefly, a mixture of PDMS oligomer  
7 83 and curing agent (Sylgard 184, Dow Corning) in a ratio of 10:1 was cast against a master to  
8 84 give a chip thickness of ~ 5 mm. This was cured at 70 °C overnight. The chip consists of two  
9 85 parallel channels at a distance of 1 mm apart. The length, width and depth dimensions of each  
10 86 channel are 13 mm × 500 µm × 500 µm.

11 87 The thin agarose gel membrane was made from a 2% agarose solution (Sigma-Aldrich) in  
12 88 deionised water. The solution was autoclaved and stored at 4 °C prior to use. The sterilised  
13 89 agarose gel solution was melted and cast between two clean coverslips separated by a 250 µm  
14 90 thick PDMS spacer. Within 20 minutes at room temperature, the membrane formed. After  
15 91 removal of the top coverslip and the PDMS spacer, the formed membrane was slid onto the  
16 92 channel side of an upturned PDMS chip. All the components were sterilised prior to use.

17 93 To form the monolayer of bacteria, 3 µl of a bacterial suspension (OD<sub>600</sub> in the range of  
18 94 0.05 - 0.08) was dispensed onto the centre of the agarose gel membrane, and immediately  
19 95 covered with a coverslip. This led to a monolayer of bacteria being trapped between the gel  
20 96 membrane and a coverslip substrate (Figure 1, enlarged view). The whole assembly was  
21 97 clamped in a plastic holder made in house. The operation was performed in a biological safety  
22 98 hood.  
23 99

### 24 100 **Bacterial strains and chemicals**

25 101 *E.coli* (ATCC 25922, ATCC, USA) was used as the model bacteria because of the abundance  
26 102 of reference information available. Prior to inhibition experiments, *E. coli* were cultured in  
27 103 Luria-Bertani (LB) broth in a shaker at 150 rpm at 37 °C. When the optical density of a  
28 104 bacterial suspension at 600 nm (OD<sub>600</sub>) reached about 0.6 - 0.8, indicating the exponential  
29 105 growth stage, bacteria were harvested by centrifugation at 5000 rpm for 1 min, washed three  
30 106 times with phosphate buffer saline (PBS) and re-suspended in fresh LB broth. The bacterial  
31 107 suspension was diluted to reach an OD<sub>600</sub> value of about ~0.08 for inhibition tests on the  
32 108 microfluidic device.

33 109 *Comamonas denitrifican* (ATCC 700936, ATCC, USA) is a denitrifying bacterium isolated  
34 110 from activated sludge known for its unique properties of reducing nitrate to nitrogen gas both  
35 111 in aerobic and anaerobic conditions<sup>16</sup>. It can be used in a toxicity assay of wastewater. Prior to  
36 112 inhibition experiments, bacteria were cultured in nutrient broth in a shaker at 150 rpm under  
37 113 30 °C. The following procedures are same as *E.coli* for the tests on the microfluidic device.

38 114 Amoxicillin (MW=419.46 Da, Sigma-Aldrich) was prepared as a 2.0 g/L stock solution in  
39 115 deionised water and then diluted in LB broth or nutrient broth to the required concentration.  
40 116

### 41 117 **On-chip bacterial growth inhibition tests**

42 118 On chip inhibition tests were conducted by delivering “source” and “sink” solutions through  
43 119 the two parallel channels in the chip (Figure 1). The solutions were continuously delivered  
44 120 into the chip at a speed of 5 µL/min (i.e. linear velocity of 0.33 µm/s within the source and  
45 121 sink channels) by a syringe pump (NE-4000, Newera Pump Systems Inc.). The continuous  
46 122 flow culture provided constant nutrient supply and removal of metabolic waste. A solution of

1  
2  
3 123 5 mg/L amoxicillin in the appropriate broth for each bacteria was used as the “source” and a  
4 124 blank broth as the “sink”. All experiments were performed at room temperature (~22°C), in  
5 125 line with a commonly found habitat temperature for bacteria in the environment. At least  
6 126 three replicate experiments were conducted for each of the conditions reported below.  
7  
8 127

### 9 128 **Image and data processing**

10 129 Time-lapse image acquisition was carried out using an inverted fluorescence microscope  
11 130 (Zeiss AxioObserver Z1) equipped with an automated stage and a 40x objective lens. Images  
12 131 were captured using a CCD camera (Photometrics Cascade II). Bright field images of the  
13 132 monolayer of bacteria were taken during the inhibition tests on chip. Large areas of the device  
14 133 (e.g. 1.5 mm × 1.5 mm) were imaged by tiling. A Matlab program was applied to stitch tiled  
15 134 pictures together to cover the whole area between the two channels. All the images were  
16 135 processed with Image J. Auto-contrast was applied to bright field images, which gave rise to  
17 136 clearly defined cell edges. For calculating cell areas, bright field images were first background  
18 137 subtracted and then converted into binary (black and white) images. Finally, the areas of each  
19 138 colony were calculated using the ‘analyzing particle’ function in Image J with a circularity  
20 139 parameter of 0-1 and particle size from 0-infinity, with the answers being given in terms of  
21 140 the number of pixels. Cell numbers within the colonies were counted manually.  
22 141

### 23 142 **Calculation of bacterial growth rates.**

24 143 Bacterial growth rate is defined as the increment ratio of a population, which can be measured  
25 144 by the increment in cell mass or in viable cell number. Since bacteria grow as a non-confluent  
26 145 monolayer on chip, cell mass in a colony can be considered to be directly proportional to the  
27 146 colony’s area.<sup>28</sup> Therefore, in the exponential increment phase of the bacteria, the growth  
28 147 rates of the bacteria from cell mass can be determined by Equation 1.<sup>29</sup>

$$29 148 \quad \ln R_M = \ln(S / S_0) = \mu_M(t - t_M) \quad (\text{Equation 1})$$

30 149 Where  $R_M$  is the increment ratio based on cell mass.  $S_0$  and  $S$  are cell area at the initial time  
31 150 ( $t = 0$ ) and at time  $t$ , which are represented by the bacterial colony areas on the chip.  $\mu_M$  is the  
32 151 specific growth rate ( $\text{h}^{-1}$ ) associated with cell mass.  $t_m$  is the lag period of bacteria growth  
33 152 associated with cell mass.

34 153 The growth rates from the exponential increment in cell number ( $R_N$ ) can be calculated by  
35 154 Equation 2, which is independent of cell morphological variations.

$$36 155 \quad \ln R_N = \ln(N / N_0) = \mu_N(t - t_N) \quad (\text{Equation 2})$$

37 156 Where  $R_N$  is the increment ratio based on cell number,  $N_0$  and  $N$  are cell numbers in the  
38 157 colony at the initial time ( $t = 0$ ) and at time  $t$ .  $\mu_N$  is the specific growth rates ( $\text{h}^{-1}$ ) associated  
39 158 with cell number.  $t_N$  is the lag period of bacterial growth associated with cell number.  
40 159

### 41 160 **Evaluation of inhibition response and IC50.**

42 161 Inhibition rates were commonly used to characterize the inhibitory response for different  
43 162 levels of exposure to an inhibitor, and were determined by the reduced specific growth in  
44 163 comparison to a control (Equation 3).<sup>30</sup>

$$45 164 \quad IR = (\mu_0 - \mu_C) / \mu_0 \quad (\text{Equation 3})$$

1  
2  
3 where  $IR$  is the inhibition rate,  $\mu_C$  and  $\mu_0$  are the specific growth rates at concentration  $c$  and  
4 in the absence of antibiotics respectively. The resultant concentration - inhibition rate curves  
5 can be fitted with a logistic model,<sup>29, 31</sup> shown in Equation 4, to represent and predict the  
6 antibiotic resistance capability of the population.  
7

$$169 \quad IR = a / [1 + (C / C_0)^b] \quad (\text{Equation 4})$$

170 Where  $a$ ,  $b$  and  $C_0$  are constants. If  $a$  is equal to 1, then  $C_0$  is equivalent to the IC50, i.e.  
171 the antibiotic concentration that is half that required to inhibit growth completely ( $IR = 0.5$ ).  
172

## 173 RESULTS AND DISCUSSION

### 174 Growth rates from cell number and cell mass without antibiotic inhibition

175 It is well known that bacteria can change their morphology under environmental stress,<sup>14</sup> thus  
176 we evaluated the growth parameters based on both cell mass and on viable cell number in  
177 normal growth medium first. Time-lapse images of a monolayer of bacteria trapped between a  
178 porous agarose gel membrane and a cover glass were collected for 6 hours. As a consequence  
179 of having a single-layer culture, high resolution images could be readily obtained during the  
180 course of the culture (Figure 2). Individual cells within the colony were clearly  
181 distinguishable, allowing manual counting of cell number.

182 Without amoxicillin ( $C_{AM} = 0$  mg/L), no obvious morphological changes occurred during  
183 the course of culture. The majority of rod-like shaped cells maintain a constant width (Figure  
184 S1, supporting information), although individual length varies between 3 to 11  $\mu\text{m}$  due to cell  
185 division. The specific growth rate from cell mass  $\mu_M$  is  $0.91 \text{ h}^{-1}$ , similar to that from cell  
186 number  $\mu_N$  ( $0.96 \text{ h}^{-1}$ ), suggesting that the two methods are comparable for calculating the  
187 growth rates. The lag time calculated from cell numbers,  $t_N$ , is 2.05 h. This is longer than that  
188 calculated from cell mass measurements,  $t_M$  (1.35 h). This discrepancy reflects the influence  
189 of cell generation on the two methods. During the process of cell generation, cell mass  
190 increases continuously whereas cell numbers increase periodically, after cell division.  
191

### 192 Quantification of antibiotic inhibition based on cell number and on cell mass

193 Previously, we showed that a stable gradient of amoxicillin forms 20 minutes after delivery of  
194 the “source” (i.e 5 mg/L amoxicillin solution) and the “sink” (a blank medium) solutions to  
195 the microfluidic channels in the PDMS chip.<sup>27</sup> At a constant flow rate of 0.33 mm/s, the  
196 gradient profile was stable for hours to days (Figure S2 and video 1, supporting information),  
197 allowing long-term evaluation of antibiotic inhibition on cells. The overall image of the  
198 bacterial monolayer between the two channels obtained via tiling provided the spatial  
199 distribution of bacteria, and thus enabled quantitative evaluation of amoxicillin’s effect for the  
200 whole range of concentrations within the gradient.

201 Cell morphology variations were observed under amoxicillin inhibition, showing  
202 dependency on both amoxicillin concentrations and time scales. A hierarchy process of  
203 elongation (i.e. filamentation), bulging, lysis and dissolution was found during the killing  
204 (Figure 3A). This phenomenon showed that cell division could be inhibited prior to the  
205 inhibition of metabolic activity. Therefore, the numbers of cells did not increase despite the  
206 continuous increase in total cell mass within a colony. This led to a discrepancy in calculating  
207 the growth rate from cell number  $\mu_N$  and that from cell mass  $\mu_M$ .

1  
2  
3 208 As shown in Figure 3B, with the increase of amoxicillin concentrations and period of  
4 209 treatment, both growth rates decreased and the deviations between them became increasingly  
5 210 apparent. Since the variations were prominent in the late period of treatment, growth rates  
6 211 between time 4 h and 6 h were given for comparison (Figure 3B). At a low concentration (e.g  
7 212  $C_{AM} = 1.4$  mg/L), growth rates of  $\mu_N$  ( $0.94$  h<sup>-1</sup>) and  $\mu_M$  ( $0.81$  h<sup>-1</sup>) are still comparable. At  
8 213 higher concentrations (e.g  $C_{AM} = 2.3$  mg/L),  $\mu_N$  ( $0.23$  h<sup>-1</sup>) reduced to about 40% value of  $\mu_M$   
9 214 ( $0.52$  h<sup>-1</sup>). A further increase of amoxicillin concentration led to substantial cell lysis and a  
10 215 rapid reduction in cell generation after 3 hours exposure and consequently a decay stage in the  
11 216 growth curve (i.e the negative increment region in Figure 3B,  $C_{AM} = 2.5$  mg/L). In contrast,  
12 217 the growth curve derived from cell mass (even at  $C_{AM} = 3.3$  mg/L) does not have such an  
13 218 abrupt transition. This is principally because the time required for a lysed cell to be dissolved  
14 219 leads to a gradual loss in cell mass. This suggests that growth curves from cell number could  
15 220 reflect the inhibitory function of antibiotic more dramatically and rapidly.

16 221 Despite growth rates based on mass and numbers having different absolute values for the  
17 222 same conditions, the deviations were systematic across the whole range of concentrations.  
18 223 The half maximal inhibitory concentration (IC50) is often used to describe the effectiveness  
19 224 of an inhibitor and was derived from the logistic function (Equation 4) fitting of concentration  
20 225 - inhibition rate curves (Figure 4). The inhibition curve from cell number ( $IR_N$ ) was slightly  
21 226 sharper than that from cell mass ( $IR_M$ ), implying its higher sensitivity in the characterisation  
22 227 of bacterial response to antibiotic inhibition. The IC50 derived from the  $IR_N$  and  $IR_M$  curves  
23 228 are 2.33 mg/L and 2.50 mg/L respectively. This shows that quantifications of antibiotic  
24 229 inhibition by both methods are in a good agreement.  
25 230

### 231 **Single cell growth rates and morphological dynamics revealing a new form of** 232 **persistence**

233 Via tracking single cell morphological variations, it became apparent that individual cells  
234 235 responded differently to the same antibiotic stress. According to the morphology of a cell and  
236 237 its growth rates (i.e.  $\mu_N$  and  $\mu_M$ ), we were able to categorise cell responses to amoxicillin into  
238 239 five states, namely (1) fast, uninhibited normal growth; (2) elongation growth (moderately  
240 241 reduced  $\mu_N$ ); (3) slow growth (significantly reduced  $\mu_M$  and  $\mu_N$ ), (4) bulge - lysis transition  
242 243 (very low  $\mu_M$  and negative  $\mu_N$ ), and (5) cell dissolution. It was found that the majority of cells  
244 245 adopted states 1 & 2 at concentrations far below IC50 whereas states 4 & 5 prevailed at  
246 247 higher concentrations ( $C_M > 3.3$  mg/L).

248 249 Interestingly, the five states were concurrently adopted by adjacent cells at concentrations  
250 251 close to IC50. Several representative examples, designated by the numbers in Figure 5A, were  
252 253 exposed to an amoxicillin concentration of 2.4 mg/L. Cell-1 & cell-2 underwent the complete  
254 255 sequence in the killing process, as was observed for the majority of cells. Cell-3 shows a  
256 257 significantly reduced growth (i.e. state 3) throughout the 6 h antibiotic treatment, without any  
258 259 obvious morphological variations, indicating that it is a possible persister in the population.<sup>15</sup>

260 261 The most surprising phenomenon occurred with cell-4 where the killing process was  
262 263 stopped and replaced by re-growth. There, as shown in Figure 5a, cell-4 survived the first 4 h  
264 265 of antibiotic treatment by elongation growth with a slow growth rate (region I in Figure 5B).  
266 267 However, lysis of the adjacent cells, cell-1 & cell-2, occurred during this time. Since  
268 269 amoxicillin acts by damaging the cell wall, cytoplasm is released into the surrounding area.  
270 271

1  
2  
3 252 This appears to be utilised by cell-4 and its colony (arrows in Figure 5A). Fast re-growth of  
4 253 cell-4's colony was observed after time 5 hours, and had a growth rate equivalent to that  
5 254 without amoxicillin inhibition (region II in Figure 5B). This phenomenon was observed in  
6  
7 255 several other places at the concentrations close to IC50 (Figure S3, supporting information)

8 256 It should be noted that the observed phenomenon can not be described as the phenotype  
9 257 switch of a type II persister cell into a normal growing cell, since a type II persister cell grows  
10 258 at a rate that is an order of magnitude slower than a non-persister cell.<sup>15</sup> Cell-4 grew/divided  
11 259 at a comparable rate to cell-1 & cell-2 during the first 3 h of exposure, and showed its  
12 260 susceptibility to amoxicillin inhibition by filamentation at time 4 h – all indicating it is most  
13 261 likely to be a normal cell and is sensitive to amoxicillin inhibition.

14 262 To evaluate whether the released cytoplasm played a role in the fast re-growth of cell-4's  
15 263 colony, inhibition tests with and without cell lysate extract from lysed *E. coli* were conducted  
16 264 in 96 well plates (Protocol detailed in the Supporting Information). A series of amoxicillin  
17 265 concentrations in three different culture mediums, namely LB broth, cell extract in PBS, and a  
18 266 mixture of LB broth and the cell extract at a ratio of 1:1, were used. In LB broth, the reduction  
19 267 in the growth rates is clearly proportional to the amoxicillin concentrations (Figure 6A and  
20 268 Figure S4A, supporting information). In cell extract, the overall cell growth rate is  
21 269 substantially lower than in LB medium (Figure 6B and Figure S4B, supporting information).  
22 270 However, no obvious inhibition was observed for all the amoxicillin concentrations,  
23 271 suggesting the cell extract enhanced cell persistence. In the mixture of cell extract and LB, the  
24 272 growth curves at all the amoxicillin concentrations match well to that in LB only without  
25 273 amoxicillin (Figure 6C and Figure S4C, supporting information) – a phenomenon that may  
26 274 explain the restored growth rate of cell's 4 colony (region II in Figure 5B). In contrast to the  
27 275 sigmoidal shaped curve from LB broth, the inhibition rates from LB & cell extract were low  
28 276 and constant across all concentrations (Figure 6D), demonstrating that cells in these  
29 277 conditions have higher persistence to amoxicillin.

30 278 Taken together, this finding, suggests that bacterial persistence can be gained by normal  
31 279 cells that are sensitive to antibiotics if an opportunity rises. The opportunity is closely linked  
32 280 with the response of cells in its close proximity to the antibiotic stress. Clearly, the  
33 281 opportunity of utilising the cytoplasm released from lysed cells close-by seems pivotal. We  
34 282 term this acquired persistence in normal growing cells as an “opportunistic persistence”.

35 283

### 36 284 **Implication to environmental bacteria**

37 285 Denitrification is a major process in the global nitrogen cycle. In the last decade, *Comamonas*  
38 286 *denitrifican* was identified in various ecosystems and wastewater treatment plants as being a  
39 287 bacteria that plays active roles in the process.<sup>32, 33</sup> Similar to *E. coli*, in the absence of  
40 288 amoxicillin inhibition (i.e.  $C_{AM} = 0$  mg/L), *Comamonas denitrifican* growth rates  $\mu_M$  (0.40 h<sup>-1</sup>)  
41 289 and  $\mu_N$  (0.44 h<sup>-1</sup>) were comparable. Time lapse tracking the growth of *Comamonas*  
42 290 *denitrifican* under an amoxicillin concentration gradient established on chip was carried out  
43 291 for 20 hours. The occurrence of the killing process, i.e. filamentation – bulge – lysis, was  
44 292 observed at different concentrations during the course of treatment (Figure 7). The  
45 293 concentration-inhibition rate curves from both cell number (rapid, <8 h) and cell mass (~20 h)  
46 294 were obtained as described above (Figure S5, Supplementary information). The derived IC50  
47 295 from cell number is 3.6 mg/L and from cell mass is 3.8 mg/L.

48  
49  
50  
51  
52  
53  
54  
55  
56  
57  
58  
59  
60

1  
2  
3 296 Interestingly, the stimulated re-growth of the inhibited cells was also observed in  
4 297 *Comamonas denitrifican* at concentrations close to IC50 after 15 h amoxicillin treatment. As  
5 298 shown in Figure 8A, some cells in the colony (indicated by the arrow) were lysed and  
6 299 dissolved at time 16 h. This was followed by a revival of fast growth of the remaining cells in  
7 300 the colony. As a result, rather than a continuous decline in the growth rate after 16 h, an  
8 301 increase in the growth rate was observed at longer period of antibiotic treatment (e.g. at time  
9 302 20 h), as shown in Figure 8B.

10  
11  
12 303 It is well known that *Comamonas denitrifican* tends to deposit polysaccharides and form a  
13 304 biofilm in the environment.<sup>34, 35</sup> Thus, the inhibition of amoxicillin to *Comamonas*  
14 305 *denitrifican* in the environment might depend on the structure of its biofilm. In particular, the  
15 306 bacteria density within the film can be vital since it determines the spatial distance between  
16 307 adjacent cells and the penetration of antibiotics (which may consequently vary in  
17 308 concentration across the film). Antibiotic resistance of biofilms is complicated<sup>36</sup> and a  
18 309 detailed discussion is beyond the scope of this work. However, it seems clear that the  
19 310 inhibitory function of bacterial membrane targeting antibiotics, such as amoxicillin, may be  
20 311 compromised by the existence of “opportunistic persistence” in the bacterial community in  
21 312 biofilms.  
22  
23  
24  
25

## 26 314 CONCLUSIONS

27 315 Growth rates calculated from the increment in cell mass and in cell number are widely used in  
28 316 the microbiological community. Via tracking single cell morphological variations, we have  
29 317 shown that there is negligible difference between the growth rates evaluated from both  
30 318 methods at optimised growth condition. However, deviations are found when substantial  
31 319 morphological variations occur due to antibiotic stresses. These deviations are systematic, and  
32 320 consequently the IC50 values evaluated by both methods are in a good agreement.

33 321 Enabled by the quantification of the growth rates and morphological dynamics of  
34 322 individual cells, the most surprising finding in this work is that sensitive bacteria can acquire  
35 323 persistence during amoxicillin treatment if an opportunity arises. Such an “opportunistic”  
36 324 persistence is characterised by fast re-growth of inhibited bacteria, which by chance were able  
37 325 to utilise the cytoplasm leaked from lysed cells in a close proximity. As a result, the killing  
38 326 process was stopped, i.e. the inhibition of amoxicillin is compromised. Such phenomenon was  
39 327 observed in both *E. coli* and an environmental bacteria *Comamonas denitrifican*.

40 328 The discovery highlights the importance of studying the heterogeneity of bacterial  
41 329 populations and their existence as a community in the resistance to antibiotic stresses.  
42  
43  
44  
45  
46

## 47 331 ACKNOWLEDGMENT

48 332 We thank the financial support from Environmental Simulation and Pollution Control State-  
49 333 key Joint Laboratory (12L01ESPC), Tsinghua University Initiative Scientific Research  
50 334 Program (No.20121087922) and from EPSRC (EP/H04986X/1 and EP/J009121/1).  
51  
52

## 53 336 SUPPORTING INFORMATION

54 337 Figure S1. Cell width variation without antibiotic treatment. Figure S2 and Video 1.  
55 338 Concentration gradient profiles of fluorescein during the first 8 h. Figure S3. An example of  
56 339 resurrection of an inhibited *E. coli* cell at  $C_{AM} = 2$  mg/L. Figure S4: The growth curves of *E.*  
57  
58  
59  
60

1  
2  
3 340 *coli* under different inhibition conditions in 96-well plates. Protocols for inhibition  
4 341 experiments with and without cell lysate extract. Figure S5. Concentration - inhibition rate  
5 342 curves for *Comamonas Denitrifican*.  
6  
7 343

#### 8 344 REFERENCES:

- 9 345 1. J. W. Bigger, *Lancet*, 1944, 2, 497-500.  
10 346 2. R. Koczura, J. Mokracka, L. Jablonska, E. Gozdecka, M. Kubek and A. Kaznowski, *Sci. Total Environ.*,  
11 347 2012, 414, 680-685.  
12 348 3. M. Habash and G. Reid, *J. Clin. Pharmacol.*, 1999, 39, 887-898.  
13 349 4. D. M. Livermore, *Clin. Microbiol. Rev.*, 1995, 8, 557-&.  
14 350 5. C. Begot, I. Desnier, J. D. Daudin, J. C. Labadie and A. Lebert, *J. Microbiol. Methods*, 1996, 25, 225-  
15 351 232.  
16 352 6. D. E. Contois, *J. Gen. Microbiol.*, 1959, 21, 40-50.  
17 353 7. P. Dalgaard, T. Ross, L. Kamperman, K. Neumeyer and T. A. McMeekin, *Int. J. Food Microbiol.*, 1994,  
18 354 23, 391-404.  
19 355 8. C. a. L. S. Institute, <http://www.clsi.org>.  
20 356 9. J. S. Soothill, R. Ward and A. J. Girling, *J. Antimicrob. Chemother.*, 1992, 29, 137-139.  
21 357 10. J. M. Andrews, *J. Antimicrob. Chemother.*, 2001, 48, 5-16.  
22 358 11. E. G. Biesta-Peters, M. W. Reij, H. Joosten, L. G. M. Gorris and M. H. Zwietering, *Appl. Environ.*  
23 359 *Microbiol.*, 2010, 76, 1399-1405.  
24 360 12. P. Dalgaard and K. Koutsoumanis, *J. Microbiol. Methods*, 2001, 43, 183-196.  
25 361 13. K. Francois, F. Devlieghere, A. R. Standaert, A. H. Geeraerd, I. Cools, J. F. Van Impe and J. Debevere,  
26 362 *J. Appl. Microbiol.*, 2005, 99, 1503-1515.  
27 363 14. N. Dhar and J. D. McKinney, *Curr. Opin. Microbiol.*, 2007, 10, 30-38.  
28 364 15. N. Q. Balaban, J. Merrin, R. Chait, L. Kowalik and S. Leibler, *Science*, 2004, 305, 1622-1625.  
29 365 16. H. B. Yin and D. Marshall, *Curr. Opin. Biotechnol.*, 2012, 23, 110-119.  
30 366 17. H. B. Yin, N. Patrick, X. L. Zhang, N. Klauke, H. C. Cordingley, S. J. Haswell and J. M. Cooper, *Anal.*  
31 367 *Chem.*, 2008, 80, 179-185.  
32 368 18. H. B. Yin, X. L. Zhang, N. Patrick, N. Klauke, H. C. Cordingley, S. J. Haswell and J. M. Cooper, *Anal.*  
33 369 *Chem.*, 2007, 79, 7139-7144.  
34 370 19. M. R. Bennett and J. Hasty, *Nat. Rev. Genet.*, 2009, 10, 628-638.  
35 371 20. Z. Long, E. Nugent, A. Javer, P. Cicuta, B. Sclavi, M. C. Lagomarsino and K. D. Dorfman, *Lab Chip*,  
36 372 2013, 13, 947-954.  
37 373 21. Y. Wakamoto, J. Ramsden and K. Yasuda, *Analyst*, 2005, 130, 311-317.  
38 374 22. J. Choi, Y. G. Jung, J. Kim, S. Kim, Y. Jung, H. Na and S. Kwon, *Lab Chip*, 2013, 13, 280-287.  
39 375 23. J. R. Moffitt, J. B. Lee and P. Cluzel, *Lab Chip*, 2012, 12, 1487-1494.  
40 376 24. T. Ahmed, T. S. Shimizu and R. Stocker, *Nano Lett.*, 2010, 10, 3379-3385.  
41 377 25. B. Z. Ji, M. Cusack, A. Freer, P. S. Dobson, N. Gadegaard and H. B. Yin, *Integrative Biology*, 2010, 2,  
42 378 528-535.  
43 379 26. H. B. Yin, B. Z. Ji, P. S. Dobson, K. Mosbahi, A. Glidle, N. Gadegaard, A. Freer, J. M. Cooper and M.  
44 380 Cusack, *Anal. Chem.*, 2009, 81, 473-478.  
45 381 27. B. Li, Y. Qiu, H. B. Yin, A. Glidle, D. McIlvanna, Q. Luo, J. M. Cooper and H. Shi, *Anal. Chem.*, 2014,  
46 382 86, 3131-3137..  
47  
48  
49  
50  
51  
52  
53  
54  
55  
56  
57  
58  
59  
60

1  
2  
3  
4  
5  
6  
7  
8  
9  
10  
11  
12  
13  
14  
15  
16  
17  
18  
19  
20  
21  
22  
23  
24  
25  
26  
27  
28  
29  
30  
31  
32  
33  
34  
35  
36  
37  
38  
39  
40  
41  
42  
43  
44  
45  
46  
47  
48  
49  
50  
51  
52  
53  
54  
55  
56  
57  
58  
59  
60

383 28. I. Wong, S. Atsumi, W. C. Huang, T. Y. Wu, T. Hanai, M. L. Lam, P. Tang, J. A. Yang, J. C. Liao and  
384 C. M. Ho, *Lab Chip*, 2010, 10, 2710-2719.

385 29. J. F. Van Impe, F. Poschet, A. H. Geeraerd and K. M. Vereecken, *Int. J. Food Microbiol.*, 2005, 100,  
386 97-105.

387 30. M. L. Cabo, M. A. Murado, M. P. Gonzalez and L. Pastoriza, *J. Appl. Microbiol.*, 1999, 87, 907-914.

388 31. C. Ritz, *Environ. Toxicol. Chem.*, 2010, 29, 220-229.

389 32. L. Gumaelius, G. Magnusson, B. Pettersson and G. Dalhammar, *Int. J. Syst. Evol. Microbiol.*, 2001, 51,  
390 999-1006.

391 33. D. Patureau, E. Zumstein, J. P. Delgenes and R. Moletta, *Microb. Ecol.*, 2000, 39, 145-152.

392 34. S. Andersson, G. K. Rajarao, C. J. Land and G. Dalhammar, *FEMS Microbiol. Lett.*, 2008, 283, 83-90.

393 35. S. Andersson, G. Dalhammar, C. J. Land and G. K. Rajarao, *Appl. Microbiol. Biotechnol.*, 2009, 82,  
394 535-543.

395 36. C. de la Fuente-Nunez, F. Reffuveille, L. Fernandez and R. E. W. Hancock, *Curr. Opin. Microbiol.*,  
396 2013, 16, 580-589.

397

398

399

1  
2  
3 400 **FIGURE CAPTIONS:**

4 401 Figure 1. Configuration of the three-layered microfluidic device (left) and enlarged view of  
5 402 the bacteria layer (right). A steady concentration gradient of an inhibitor is established  
6 403 between the “source” and “sink” channels.

7  
8 404 Figure 2. (A) Time-lapse images of *E.coli* during 6 h culture at LB medium. Scale bar  
9 405 represents 10  $\mu\text{m}$ . (b) Growth rates of *E.coli* calculated from cell number and from cell mass  
10 406 (number of colonies,  $n=15$ ). For the clarity of the figure, only half of the error bars (standard  
11 407 deviations) are shown.

12  
13 408 Figure 3. (A) Diverse responses of *E.coli* exposed to amoxicillin. Scale bars 10  $\mu\text{m}$ . (B)  
14 409 The deviation of growth rates from cell number and cell mass with the increase in amoxicillin  
15 410 concentrations. Five adjacent colonies were selected at each amoxicillin concentrations ( $C_{AM}$ ).  
16 411 The error bars show the standard deviations.

17  
18 412 Figure 4. Inhibition curve fitting using a logistic function for *E.coli* exposed to amoxicillin.

19 413 Figure 5. (A) Time-lapse images of the acquired “opportunistic” persistence process. The  
20 414 inhibited cell-4 regained fast growth after utilising the released cytoplasm from lysed cell-1 &  
21 415 cell-2 (indicated by the arrows). Scale bar 10  $\mu\text{m}$ . (B). Growth rate ( $R_N$ ) of the cell-4 in Figure  
22 416 5 during the 6 h amoxicillin treatment. The average growth curve ( $R_N$ ) from cells without  
23 417 amoxicillin treatment was included as a reference.

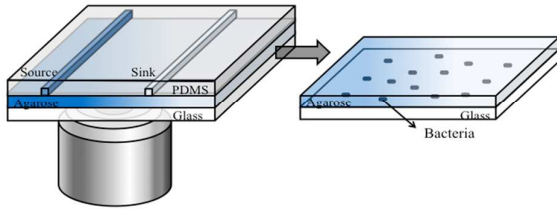
24 418 Figure 6. The effect of cell lysate extract on bacteria persistence to amoxicillin. (A, B, C)  
25 419 the growth rates of *E.coli* with and without cell extract under different amoxicillin  
26 420 concentrations in 96-well plates ( $n=3$ ). (D) The inhibition curves of *E.coli* in LB broth only  
27 421 and in the mixture of LB and cell extract. All data points have error bars of one standard  
28 422 deviation, although these are too small to be visible on some points.

29  
30 423 Figure 7. Filamentation-bulge-lysis in *Commonas denitrifican* community.

31  
32 424 Figure 8 (A) The lysis-and-regrowth in *Commonas denitrifican* community. Amoxicillin  
33 425 concentration is at 3.5 mg/L. Scale bar 10  $\mu\text{m}$ . (B) Growth rate ( $R_M$ ) of the reversed growing  
34 426 colony in (A) during the long-term period of amoxicillin treatment. The average growth rate  
35 427 of cells without amoxicillin is shown for reference.

36 428  
37 429  
38 430  
39  
40  
41  
42  
43  
44  
45  
46  
47  
48  
49  
50  
51  
52  
53  
54  
55  
56  
57  
58  
59  
60

431



432

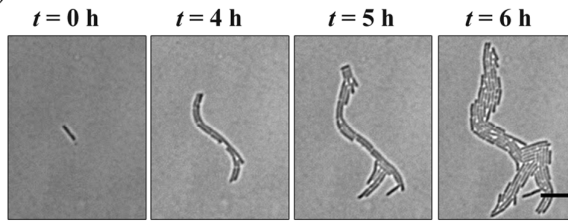
Figure 1.

433

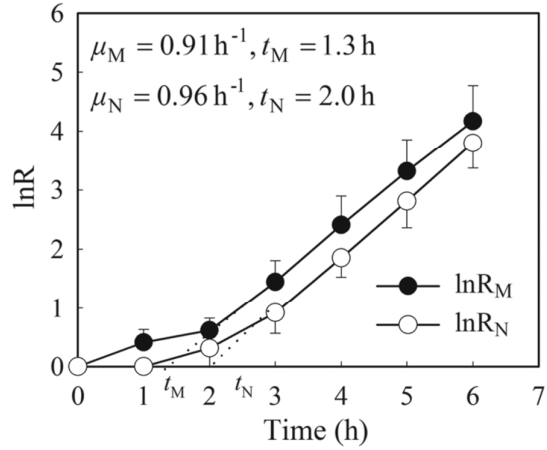
434

435

(A)



(B)



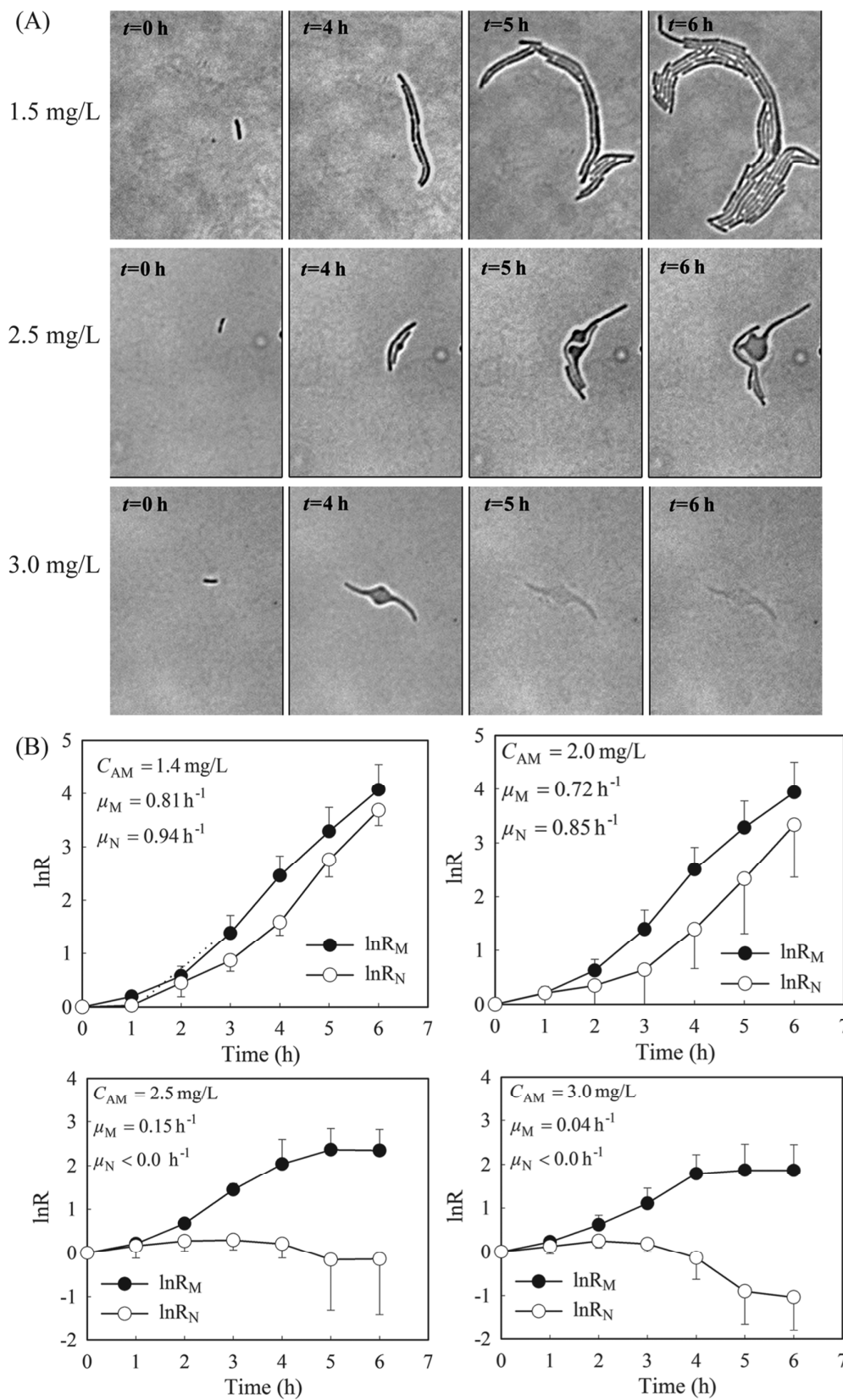
436

Figure 2.

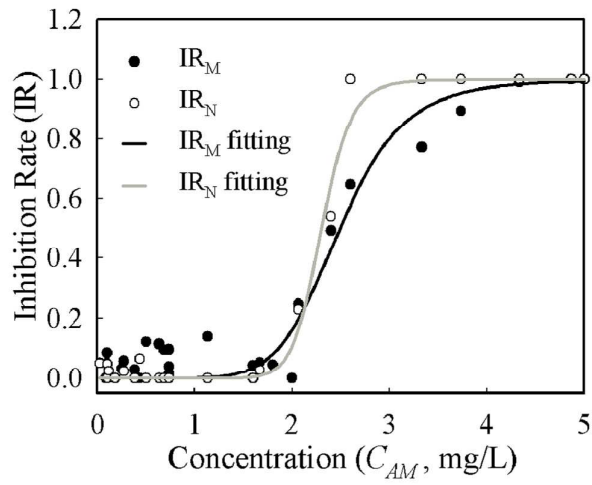
437

438

1  
2  
3  
4  
5  
6  
7  
8  
9  
10  
11  
12  
13  
14  
15  
16  
17  
18  
19  
20  
21  
22  
23  
24  
25  
26  
27  
28  
29  
30  
31  
32  
33  
34  
35  
36  
37  
38  
39  
40  
41  
42  
43  
44  
45  
46  
47  
48  
49  
50  
51  
52  
53  
54  
55  
56  
57  
58  
59  
60



441



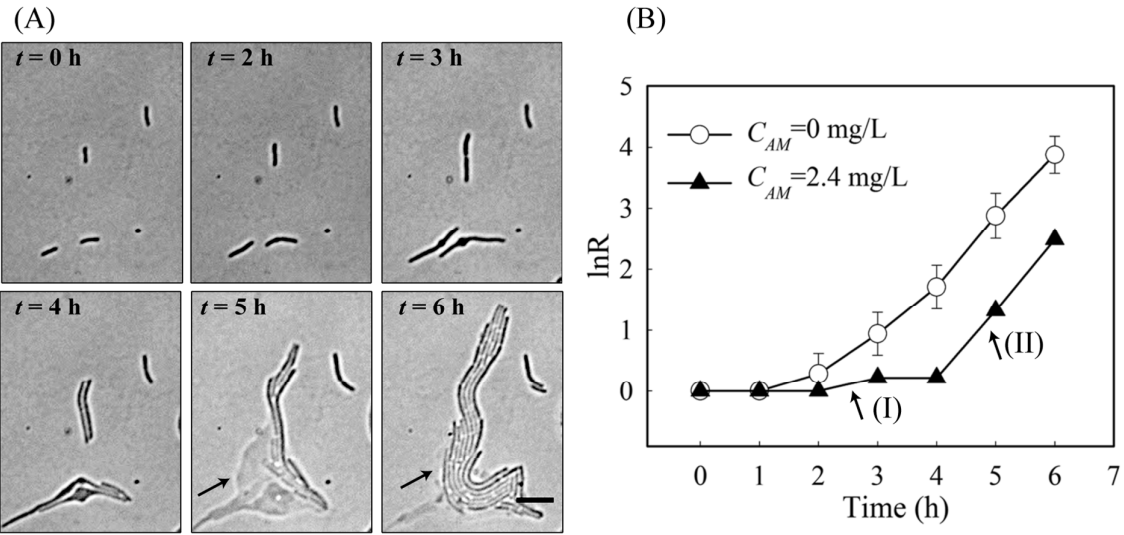
442

443 Figure 4.

444

445

446

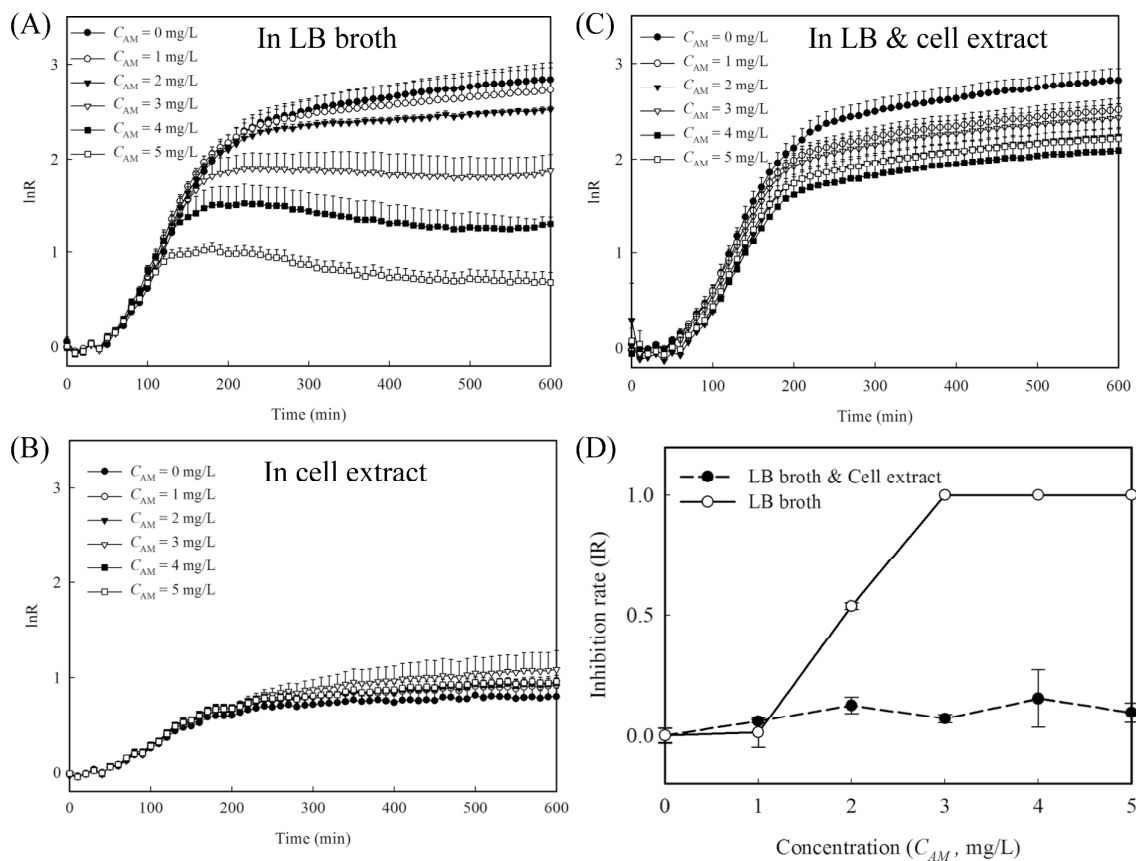


447

448

449 Figure 5.

450

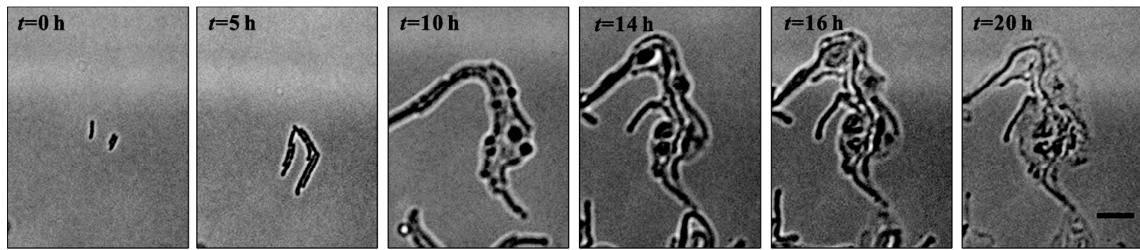


451

452 Figure 6.

453

454



455

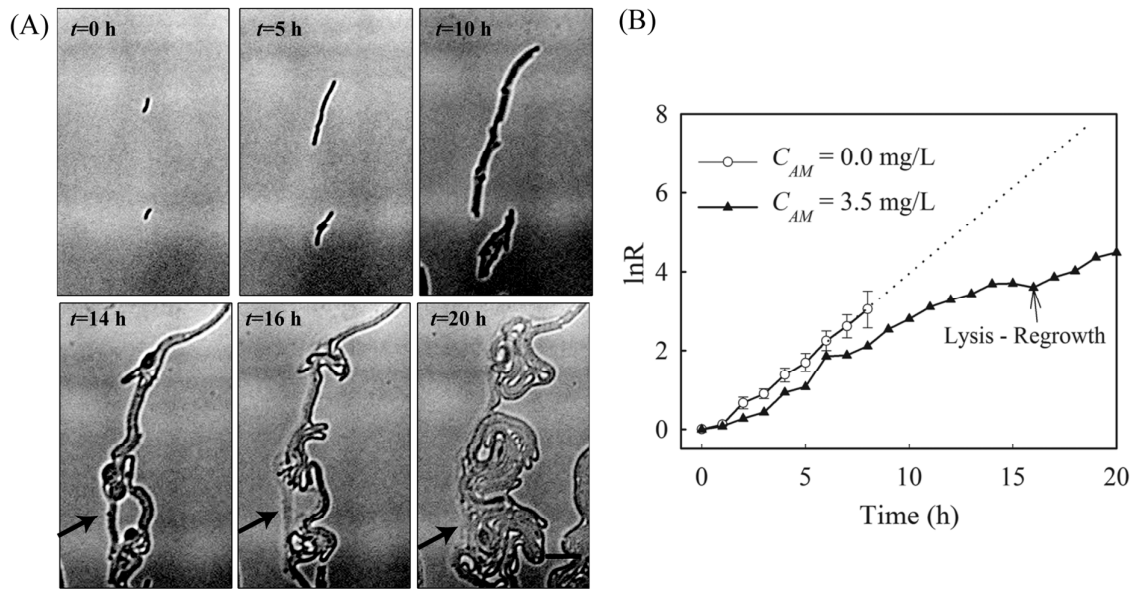
Figure 7.

456

457

458

459



460

Figure 8.

461

462

463

464

465

466

467

468

469

470

471

472

473

474

475

476

477

478

479

480

481